SCIENCE CHINA
Technological Sciences

• Article •

August 2015 Vol.58 No.8: 1360–1368
doi: 10.1007/s11431-015-5876-2

Nanoindentation analysis of TiN, TiAlN, and TiAlSiN coatings prepared by cathode ion plating

KONG DeJun[1,2*] & FU GuiZhong[1]

[1]*College of Mechanical Engineering, Changzhou University, Changzhou 213164, China;*
[2]*Jiangsu Key Laboratory of Materials Surface Science and Technology, Changzhou University, Changzhou 213164, China*

Received April 11, 2015; accepted June 17, 2015; published online July 2, 2015

The TiN, TiAlN and TiAlSiN coatings were deposited on H13 hot-worked mold steel by cathodic arc ion plating (CAIP). The morphologies, phase compositions, and nanoindentation parameters, such as creep hardness, elastic modulus and plastic deformation energy of the coatings were analyzed with field emission scanning electron microscopy (FESEM), X-ray diffraction (XRD) and nanoindentation testing, respectively, and the test results were compared with equation describing the indentation model. The results show that the TiN, TiAlN and TiAlSiN coating surfaces were dense and composed of TiN, TiN + TiAlN, TiN + Si_3N_4 + TiAlN phases, respectively. There was no spalling or cracking on the indentation surface. The creep hardness of the TiN, TiAlN and TiAlSiN coatings was 7.33, 13.5, and 15.2 GPa, respectively; the corresponding hardness measured by nanoindentation was 7.09, 15.6, and 21.7 GPa, respectively; and the corresponding elastic modulus was 201.93, 172.79, and 162.77 GPa, respectively. The contact depth and elastic modulus calculated by the indentation model were close to those of the test results, but the remaining indentation parameters showed discrepancies. The sequence of plastic deformation energy was TiN > TiAlN>TiAlSiN.

TiN, TiAlN, and TiAlSiN coatings, nanoindentation, creep hardness, elasticity modulus, plastic deformation energy

Citation: Kong D J, Fu G Z. Nanoindentation analysis of TiN, TiAlN, and TiAlSiN coatings prepared by cathode ion plating. Sci China Tech Sci, 2015, 58: 1360–1368, doi: 10.1007/s11431-015-5876-2

1 Introduction

As an air-hardening, hot-worked mold steel, H13 has good hardenability and thermal fatigue performance, it is widely used in hot extrusion, forging of non-ferrous metal, die-casting mold, etc. [1,2]. The operating temperature can only reach 500°C. In order to improve service life of the hot-worked mold, deposition of a hard coating on H13 steel by CAIP is a possible method to increase the working temperature. The deposition of TiN coating on the H13 steel surface can effectively reduce adhesive wear phenomena of the mold at high temperatures, and the working temperature can be increased to about 550°C [3]; while the deposition of TiAlN coating on the H13 steel can increase the working temperature to about 800°C [4,5]. Addition elemental Si in the TiAlN coating to form TiAlSiN coating can increase the working temperature to about 900°C [6,7]. Because the hardness of the coating has a great influence on the wear properties of the mold simultaneously, the elastic modulus reflects the strain properties. Therefore, the hardness and elastic modulus under the short-term external loads have the most important effects on the service life of the coating [8]. Related research has concentrated on the phase composition, friction and wear, high-temperature oxidation and corrosion of TiN, TiAlN and TiAlSiN coatings [9–12], but the creep hardness, elastic modulus, and plastic deformation energy of TiN, TiAlN, and TiAlSiN coatings characterized with a

*Corresponding author (email: kong-dejun@163.com)

nanoindentation test have not been reported. TiN, TiAlN, and TiAlSiN coatings were deposited on H13 hot-worked mold steel by CAIP. The morphologies, phases, and nanoindentation parameters such as creep hardness, elastic modulus, and plastic deformation energy, of TiN, TiAlN, and TiAlSiN coatings were analyzed with a field emission scanning electron microscopy (FESEM), X-ray diffraction (XRD) and nano-indentation testing, respectively, which provided an experimental basis for the application of TiN, TiAlN, and TiAlSiN coatings for H13 steel surface modification.

2 Materials and method

The substrate material was H13 steel with chemical compositions of (mass, %): C 0.32–0.45, Si 0.80–1.20, Mn 0.20–0.50, Cr 4.75–5.50, Mo 1.10–1.75, V 0.80–1.20, P and S≤0.03. It was polished by the sandpapers of 80#, 120#, 200#, 600# and 800# and metallographic sandpaper in turn to produce a surface roughness of 0.1 μm. After degreasing and sandblasting, the samples were ultrasonically cleaned in acetone solution, dehydrated with ethanol, and then dried in a thermostat oven. The coatings were conducted on a PVT coating machine. The targets of Ti/Ti with a purity of 99.99%, Ti/Al with the purity of 99.99% and Al /TiSi with a Ti content of 80% and Si content of 20% were adopted to prepare TiN, TiAlN and TiAlSiN coatings, respectively, using the following parameters: Vacuum degree of 3×10^{-4} Pa, furnace temperature of 500°C, reaction gas of N_2, plating time of 150 min and protection gas of N_2. After annealing at 180°C for 2 h, the samples were cleaned with acetone in a KQ2200DE type CNC ultrasonic cleaner to obtain the required samples. The morphologies and phases of the TiN, TiAlN and TiAlSiN coatings were analyzed with a SUPRA55 type field emission scanning electron microscope (FESEM) and D/max 2500PC type X-ray diffraction (XRD). The hardness and elastic modulus of the TiN, TiAlN and TiAlSiN coatings were measured with a nano-situ mechanical testing system, which was produced by American Heston Instruments, using a Berkovich indenter as a pressure needle with a curvature radius of 50 nm.

3 Analysis and discussion

3.1 Surface-interface morphologies

Figure 1 shows the surface morphologies of the TiN, TiAlN and TiAlSiN coatings. The TiN coating surface was relatively flat with no uncoated areas, as shown in Figure 1(a). Metal particles with a diameter of about 400 nm were presented on the coating surface, because the metal ions did not adequately react with N_2 during deposition, and pits on the surface formed by Ti metal ion bombardment on the substrate at a high bias. There were many particles with small sizes existing on the TiAlN coating surface, as shown in Figure 1(b). The TiAlSiN coating surface was roughness, and the particles had a uniform and dense structure, as shown in Figure 1(c). The surface quality sequence of the three coatings was TiAlSiN coating>TiN coating>TiAlN coating, in which the surface quality of the TiAlSiN coating

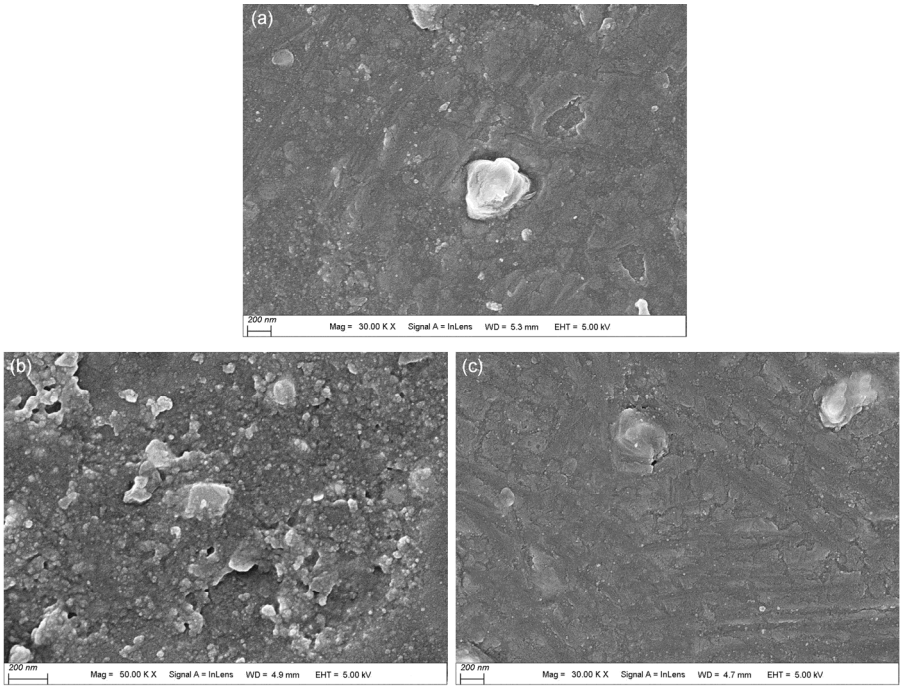

Figure 1 Surface morphologies of TiN, TiAlN and TiAlSiN coatings. (a) TiN coating; (b) TiAlN coating; (c) TiAlSiN coating.

was the best, while that of TiAlN was the worst.

As shown in Figure 2, the thicknesses of the TiN, TiAlN and TiAlSiN coatings were about 8 μm, which led to good adhesion with the substrate and uniform density. The structures of the coatings were compact without any coarse columnar grains or pores, and a fine structure was formed at the interface with the substrate.

3.2 XRD analysis

Figure 3 shows the XRD analysis results for the TiN, TiAlN and TiAlSiN coatings. The TiN coating was mainly composed of TiN phase with (111) crystal planes, as the preferred orientation, as shown in Figure 3(a). Elemental aluminum was added to the TiN coating to form a TiAlN coating. Then the coating was composed of TiAlN and TiN phases, as shown in Figure 3(b). The replacement of some of the Ti atoms of TiN phase by Al atoms produced lattice distortion, and the grain boundaries and dislocations increased to improve the hardness of the TiAlN coating. The (200) crystal plane of the NaCl-type metal nitride structure has the lowest energy, but the induced growth of the (200) crystal plane by ion bombardment with heavy atoms is harder than light atoms; therefore, the TiAlN and TiN coatings exhibited a preferred orientation along the (111) planes, but the results would differ with preparation method [13,14]. Figure 3(c) shows the grain refinement phenomenon [15] produced after elemental Si was added into the TiAlN coating to form the TiAlSiN coating. This coating was mainly composed of TiN, Si_3N_4 and TiAlN, in which Si_3N_4 and TiAlN were hard phases. Si_3N_4 can change into wearable SiO_2 phase at high temperature, which can effectively improve the hardness and wear resistance of the coating.

Figure 4 shows that the curve of pressure loading vs load in the nanoindentation with the trapezoidal loading method, where the maximum load is 2000 μN, the time is 15 s, and the indenter type is Berkovich. By keeping the load < 1 μN in the time period of 0–1.5 s, the initial contact zero of the pressure needle and coating surface was determined for the subsequent testing equipment to determine the indentation depth. In the time period of 1.5–6.5 s, the load increased from 0 to 2000 μN, and the loading rate was 400 μN/s, in the time period of 6.5–11.5 s, the maximum load was maintained for 5 s to eliminate the thermal drift of the indenter [16]. Then, the indenter was withdrawn at a rate of 400 μN/s starting at 11.5 s, and the load was 0 at 16.5 s.

3.3 Indentation curves

Figure 5 shows the nanoindentation curves of the TiN, TiAlN and TiAlSiN coatings. The load depth increased in a nonlinear manner with the load. When the load reached the maximum F_{max}=2000 μN, the maximum indentation depth was h_{max}; as the load decreased during the withdrawal, the sample elastically deformed, and the indentation depth also decreased. When the load reached 0, the indentation depth was the residual indentation depth h_f. The energy by indentation loading reflected the material volume change under the force, the area enclosed by loading curve and the horizontal axis was total work W_{total}. The area enclosed by unloading curve and the horizontal axis was elastic deformation work $W_{elastic}$, and the area enclosed by the loading

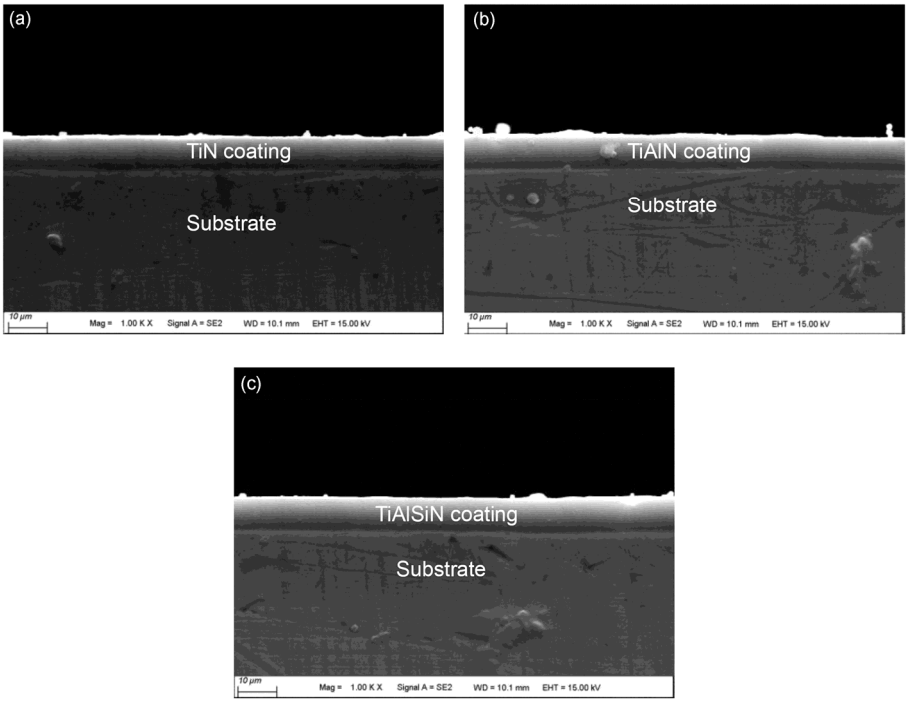

Figure 2 Interface morphologies of TiN, TiAlN and TiAlSiN coatings. (a) TiN coating; (b) TiAlN coating; (c) Morphology of TiAlSiN coating.

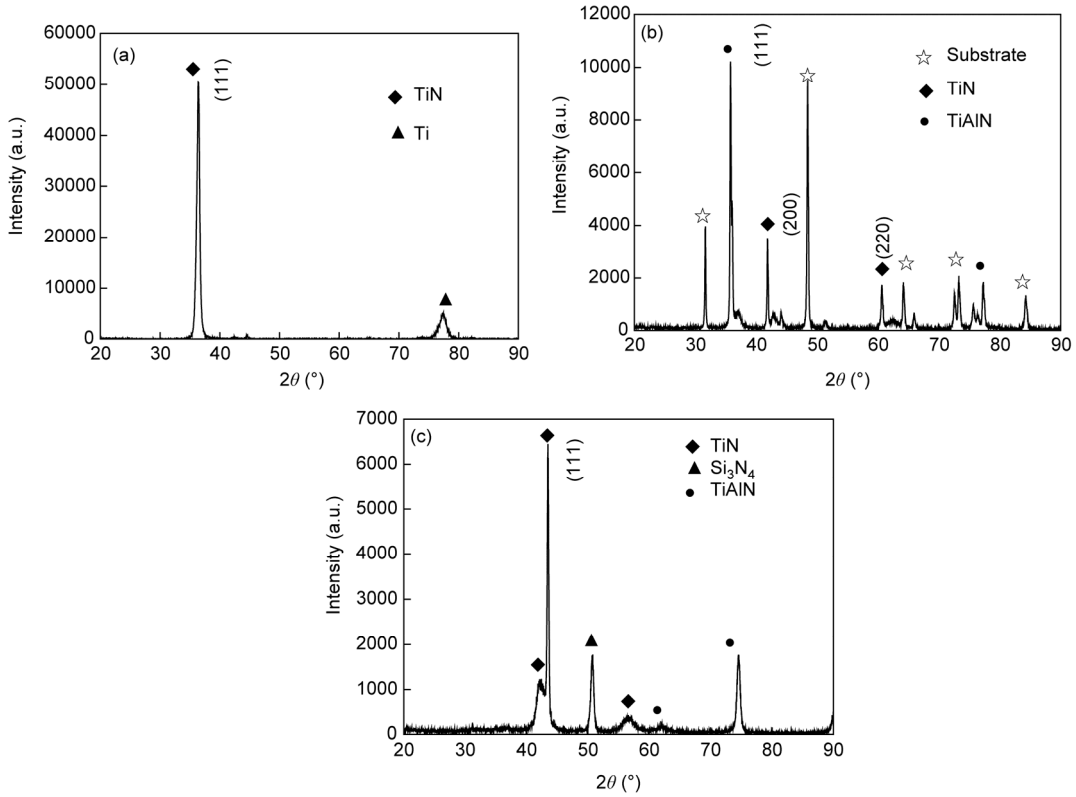

Figure 3 XRD analysis of TiN, TiAlN and TiAlSiN coatings. (a) TiN coating; (b) TiAlN coating; (c) TiAlSiN coating.

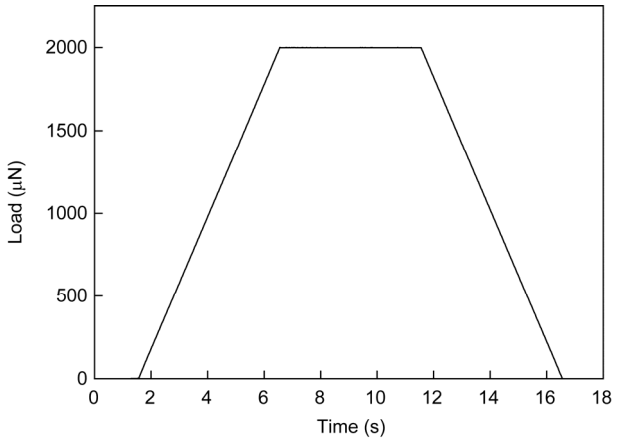

Figure 4 Pressure loading curve in nanoindentation.

curve and the unloading curve was the plastic deformation work $W_{plastic}$, which can be calculated by quadratic polynomial fitting [17]. As the indentation curves showed in Figures 5(a)–(c), the creep phenomenon appeared. When the coatings were subjected to a constant load, the indentation depth deepened. The creep displacement was the platform width of *AB* (h_{max}–h_m) in Figure 5(a), *CD* in Figure 5(b) and *EF* in Figure 5(c), where the creep displacements of the TiN, TiAlN and TiAlSiN coatings was 4.29, 4.16, and 4.88 nm, respectively.

The material creep stiffness was calculated by using the energy method [18]

$$H_{creep} = \frac{W_{cr}}{\Delta V_{cr}}, \tag{1}$$

where W_{cr} is the creep power and ΔV_{cr} is the volume change.

Here

$$W_{cr} = F_{max}\left(h_{max} - h_m\right), \tag{2}$$

where F_{max} is the maximum load value, F_{max}=2000 μN, h_{max} is the maximum indentation depth and h_m is the maximum indentation depth when creep did not occur.

$$\Delta V_{cr} = \frac{g}{3}\left(h_{max}^3 - h_m^3\right), \tag{3}$$

where g = 24.56.

The creep stiffness of the TiN, TiAlN and TiAlSiN coatings was 7.33, 13.5, and 15.2 GPa, respectively, as calculated by eqs. (1)–(3). The creep resistance sequence was TiAlSiN > TiAlN > TiN, and the creeping phenomenon was produced by dislocation creep and diffusion creep [19].

3.4 Indentation parameters

The indentation calculation model was first proposed by WC Oliver and GM Pharr in Cambridge in 1992 [20]. Figure 6 shows the various parameters and calculated values in

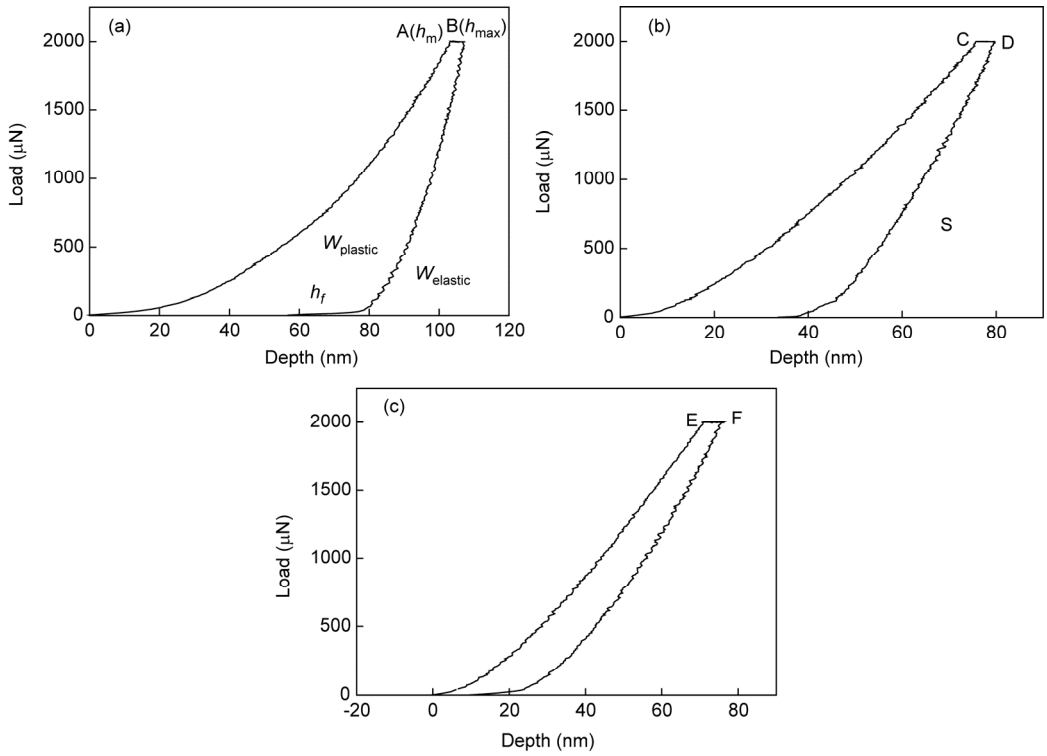

Figure 5 Indentation curves of TiN, TiAlN and TiAlSiN coatings. (a) TiN coating; (b) TiAlN coating; (c) TiAlSiN coating.

accordance with the relevant model measured by indentation testing. The maximum indentation depth, h_{max}, and residual indentation depth, h_f, were measured by the impressor, as shown in Figure 6(a). The sequence of the maximum indentation depth, h_{max}, and residual indentation depth, h_f, was TiN > TiAlN > TiAlSiN. The value of h_f/h_{max} was 0.68, 0.50 and 0.23, respectively, while the sequence of plastic deformation size was TiN > TiAlN > TiAlSiN. In Figures 5(a)–(c), the relationship between load and displacement may fit an exponential function [20,21], as eq. (4) shown, and eqs. (5)–(7) show the fitting results.

Indentation load is

$$F = a\left(h - h_f\right)^b, \tag{4}$$

where a is a constant, h is the indentation depth; h_f is the residual indentation depth and b is a constant.

By eq. (4), the TiN curve equation of the loading-indentation depth is

$$F_1 = 1.27\left(h - 73.05\right)^{2.08}. \tag{5}$$

The TiAlN curve equation for the loading-indentation depth is

$$F_2 = 10.12\left(h - 39.65\right)^{1.43}. \tag{6}$$

The TiAlSiN curve equation for the loading-indentation depth is

$$F_3 = 2.52\left(h - 17.72\right)^{1.64}. \tag{7}$$

The tangent slope of curve in the maximum depth of the indentation (*D* point) was the maximum depth of the indentation contact stiffness value [20,22], i.e.,

$$S = \left[\frac{\mathrm{d}f}{\mathrm{d}h}\right]_{h=h\,\max}. \tag{8}$$

The S value obtained from the curve fitting and calculation and the data obtained from indentation test are shown in Figure 6(b). The sequence of contact stiffness was TiN > TiAlSiN > TiAlN. The calculated and experimental values of TiN and TiAlN tended to agree, while the two values for TiAlSiN were quite different.

The contact depth of the coating is [20,21]

$$h_c = h_{\max} - \frac{\varepsilon F_{\max}}{S}, \tag{9}$$

where ε=0.75, F_{max}=2000 μN and S is the contact stiffness given in eq. (8).

The sequence of contact stiffness was TiN > TiAlN > TiAlSiN according to the calculated values and experimental values measured by the indentation testing. The calculated and experimental data tended to fit as Figure 6(c) shows.

The indentation contact area of the coating is [20]

$$A_c = 24.5h_c^{\,2} + C_1h_c^{1} + +C_2h_c^{1/2} + C_3h_c^{1/4} + \cdots + C_8h_c^{1/128}, \tag{10}$$

where C_1 to C_8 are constants and h_c is contact depth given in

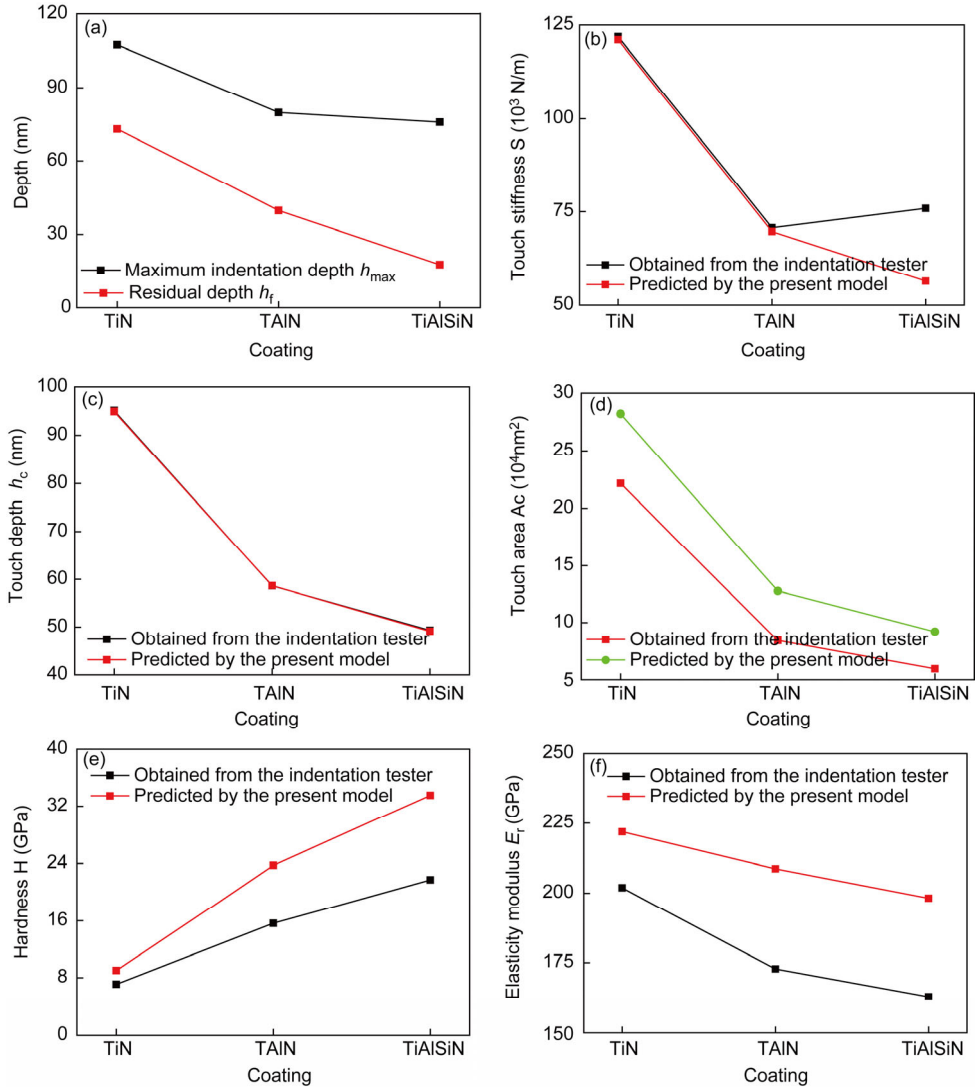

Figure 6 Nanoindentation parameters of TiN, TiAlN and TiAlSiN coatings. (a) Maximum depth and residual depth; (b) contact stiffness; (c) contact depth of indentation; (d) contact area; (e) hardness; (f) elasticity modulus.

eq. (9).

When using the standard Berkovich indenter, eq. (10) only retains the first term. When the indenter is passivated after repeated usage, a correction term is needed to be affiliated, where the indenter is considered as a standard indenter. Figure 6(d) shows that the calculated values and contact area test values given by the indentation testing, indicating that the sequence of the contact area was TiN > TiAlN > TiAlSiN. The difference between the calculated value and experimental value was 21%, 34%, and 35%, respectively, which was larger due to the indenter passivation.

The coating hardness is [20]

$$H = \frac{F_{\max}}{A_c}, \tag{11}$$

where F_{max}=2000 μN and A_c is indentation contact area given in eq. (10).

The hardness value of TiN, TiAlN and TiAlSiN coatings measured by the indentation testing was 7.09, 15.6, and 21.7 GPa, respectively. The test values and calculated values are shown in Figure 6(e). The sequence of hardness was TiAlSiN > TiAlN > TiN, and the difference between the calculated values and experimental values was 22%, 34%, and 35%, respectively. According to eqs. (8)–(11), $H \propto 1/h_{max}^2$, the higher hardness H of the coating was, the smaller h_{max} was, and the bigger the difference was. The thickness of TiN, TiAlN and TiAlSiN coatings was about 8 μm, the corresponding h_{max} was 107.4, 79.6, and 75.9 nm, respectively, and the corresponding value of h_{max}/coating thickness was 1.3%, 1%, and 0.9%, respectively. According to the results of Botero [4], the effect of h_{max}/coating thickness value had little effect on the measurement of coating hardness and elastic modulus.

The elastic modulus of the coating is

$$E_r = \frac{\sqrt{\pi}}{2\beta}\frac{S}{\sqrt{A_c}}, \tag{12}$$

where $\beta = 1.034$.

The elastic modulus value of the TiN, TiAlN, and TiAlSiN coatings measured by the indentation testing was 201.93, 172.79, and 162.77 GPa, respectively, Figure 5(f) shows the calculated values and test values given by the indentation testing. The sequence of elastic modulus values was TiN > TiAlN > TiAlSiN, and the difference between the calculated value and experimental value was 8.9%, 17.2%, and 17.8%, respectively.

3.5 Power of plastic deformation

During nanoindentation, the total power W_{total} is the sum of the elastic deformation power W_{elastic} and the plastic deformation power W_{plastic} [17,23]. The total power is

$$W_{\text{total}} = \int_0^{h\max} F_a \mathrm{d}h, \tag{13}$$

where $h_{\max}$ is the maximum indentation depth, F_a is the load and h is the indentation depth.

In eq. (13), the load is

$$F_a = 24.5Hf^2h^2, \tag{14}$$

where H is the coating hardness, f is the contact depth factor and h is the indentation depth.

In eq. (14), the contact depth factor is

$$f = 1.06\times10^{-2}\frac{h_{\max}}{h_{\max}-h_f} + 1.00, \tag{15}$$

where $h_{\max}$ is the maximum indentation depth and h_f is the residual indentation depth.

The elastic deformation power is

$$W_{\text{elastic}} = \int_{h_f}^{h_{\max}} F_b \mathrm{d}h. \tag{16}$$

In eq. (16), the uninstall load was

$$F_b = \frac{2\tan\theta}{\pi}E_r\left(h-h_f\right)^2, \tag{17}$$

where θ is the angle between the central axis and facets, θ=65.3°, E_r is the elastic modulus of the coating, h is the indentation depth and h_f is the residual indentation depth.

The shaping deformation power is

$$W_{\text{plastic}} = W_{\text{total}} - W_{\text{elastic}}. \tag{18}$$

Figure 7 shows that the data obtained by software direct integration and quadratic fitted calculation of TiN, TiAlN, and TiAlSiN coatings, which leads to the following observations. (1) The value of the total power calculated by eq. (13) was 7.66×10^{-11}, 6.78×10^{-11}, and 7.75×10^{-11} J, respectively, while the direct integration value was 7.19×10^{-11}, 6.60×10^{-11}, and 6.70×10^{-11} J, respectively, Thus, the total power obtained by calculation was consistent with the results obtained by direct integration. (2) The value of total power calculated by eq. (16) was 3.79×10^{-12}, 5.18×10^{-12}, and 1.48×10^{-11} J, respectively, while the direct integration value was 2.27×10^{-11}, 3.39×10^{-11}, and 4.4×10^{-11} J, respectively. Thus the total power obtained by calculation was different than the results obtained by direct integration. (3) The value of the total power calculated by eq. (16) was 7.28×10^{-11}, 6.26×10^{-11}, and 6.2693×10^{-11} J, respectively, while the direct integration value was 4.92×10^{-11}, 3.21×10^{-11}, and 2.29×10^{-11} J, respectively. The sequence of plastic deformation powers of the three coatings was TiN > TiAlN > TiAlSiN. The materials with good plastic performance can store more strain energy, hindering crack initiation, and propagation to improve the service life of the coatings [8].

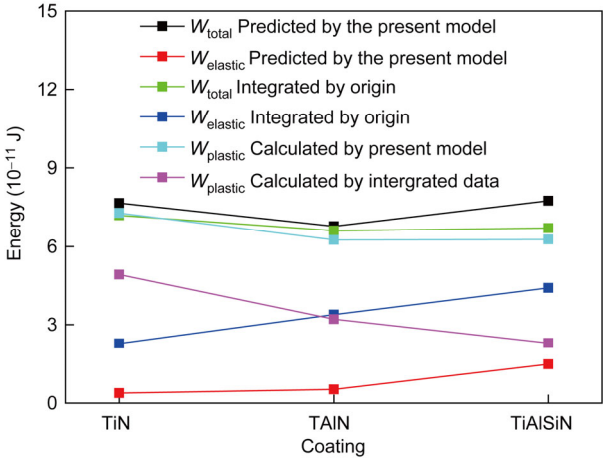

Figure 7 Total, elastic deformation and plastic deformation powers of TiN, TiAlN and TiAlSiN coatings.

3.6 Indentation morphologies

Figure 8 shows that the indentation morphologies of the TiN, TiAlN, and TiAlSiN coatings. The indentation sizes of TiN and TiAlN were greater than that of TiAlSiN, because that the hardness of the TiAlSiN coating was so high that the indenter was impressed hard. No spalling occurred on the three coating surfaces, showing that the coatings had good adhesion with the substrate of H13 steel. No cracks appeared on the surfaces of the three coatings either, showing that the coatings had good bearing capacity under the load [24]. The coating indentations were relatively smooth, which prevented the indentation of the load on the elemental phase and reduced the maximum stress of the coating. The coating exhibited homogeneous mechanical response during the indentation.

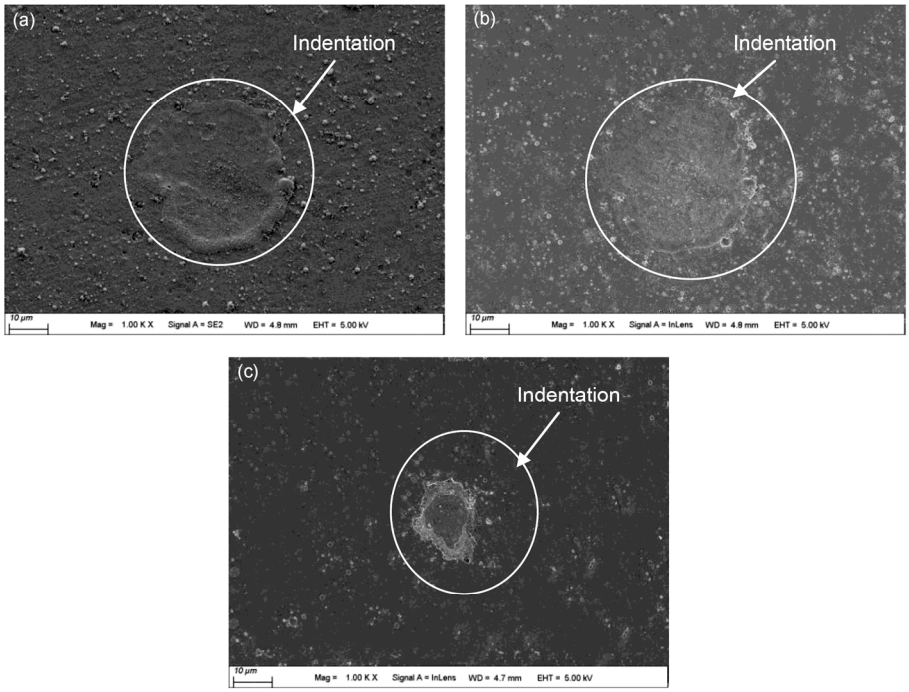

Figure 8 Nanoindentation morphologies of TiN, TiAlN and TiAlSiN coatings. (a) TiN coating; (b) TiAlN coating; (c) TiAlSiN coating.

4 Conclusions

(1) The TiN coating is mainly composed of TiN phase, and the TiAlN coating is mainly composed of TiAlN and TiN phases. The two coatings exhibit the preferred orientation of the (111) crystal plane, while the TiAlSiN coating was mainly composed of TiN, Si_3N_4 and TiAlN phases.

(2) The creep displacement of the TiN, TiAlN, and TiAlSiN coatings was 4.29, 4.16, and 4.88 nm, respectively, and the corresponding creep stiffness was 7.33, 13.5, and 15.2 GPa, respectively. The sequence of creep resistances was TiAlSiN > TiAlN > TiN due to dislocation creep and diffusion creep.

(3) The hardness value of the TiN, TiAlN, and TiAlSiN coatings was 7.09, 15.6, and 21.7 GPa, respectively, and the corresponding elastic modulus was 201.93, 172.79, and 162.77 GPa, respectively. The calculated values of the contact depth h_c and elastic modulus E_r were similar to the test values, but the other indentation parameters differed significantly.

(4) The plastic deformation power of the TiN, TiAlN, and TiAlSiN coatings obtained by direct integration of the indentation curve was 4.92×10^{-11}, 3.21×10^{-11}, and 2.29×10^{-11} J, respectively, while that by calculation was 7.28×10^{-11}, 6.26×10^{-11}, and 6.2693×10^{-11} J, respectively. The differences are bigger, and the sequence of plastic deformation power was TiN > TiAlN > TiAlSiN, in which the plastic deformation of the TiN coating was the best.

(5) The indentation morphologies of the TiN, TiAlN, and TiAlSiN coatings were relatively flat, had no peeling and cracks, and the carrying capacities were good. The hardness of TiAlSiN coating was the highest, and the indentation size was the smallest.

This work was supported by the Jiangsu Province Science and Technology Support Program (Industry) (Grant No. BE2014818).

1 Song W W, Min Y G, Wu X C. Study on carbides and their evolution in H13 hot work steel. Trans Mater Heat Treat, 2009, 30: 122–126
2 Zhang H, Xu X G, Fei X Y, et al. Effect of CrTiAlN coatings on oxidation behaviour of H13 steel at 800°C and 900°C. J Synth Cryst, 2013, 42: 2715–2719
3 Alan X, Christian B, David E J A, et al. Ion-irradiation-induced clustering in W–Re and W–Re–Os alloys: A comparative study using atom probe tomography and nanoindentation measurements. Acta Mater, 2015, 87: 121–127
4 He Z H, Qian C X, Zhang Y, et al. Nanoindentation characteristics ofcement with different mineral admixtures. Sci China Tech Sci, 2013, 56: 1119–1123
5 Xu Y C, Chen K H, Wang S Q , et al. Oxidation and cutting properties of TiN and TiAlN coated cemeted carbide. Mater Eng Powder Metall, 2011, 16: 425–430
6 Chang Y Y , Yang S M. High temperature oxidation of multicomponent TiAlSiN coating. Thin Solid Film, 2010, 518: 34–37
7 Xie Z W, Wang L P, Wang X F, et al. Influence of oxidation on the structural and mechanical properties of TiAlSiN coatings synthesized by multi-plasma immersion ion implantation and deposition. Nucl Instrum Meth B, 271: 1–5
8 Liang J J, Wei H, Hou G C, et al. Progress in mechanical and physical properties of high-temperature coating materials. Rare Met Mater Eng, 2008, 37: 1134–1138
9 He Z H, Qian C X, Zhang Y, et al. Nanoindentation characteristics ofcement with different mineral admixtures. Sci China Tech Sci, 2013, 56: 1119–1123

10 Francisco G F, Emanuele B, Angelica C, et al. The mechanical properties of a nanocrystalline Al_2O_3/a-Al_2O_3 composite coating measured by nanoindentation and Brillouin spectroscopy. Acta Mater, 2013, 61: 2662–2670
11 Han J D, Pan G H, SUN W, et al. Application of nanoindentation toinvestigate chemomechanical properties change of cement paste in the carbonation reaction. Sci China Tech Sci, 2012, 55: 616–622
12 Dipen Y, Patel K, Hamad F, et al. Extracting single-crystal elastic constants from polycrystalline samples using spherical nanoindentation and orientation measurements. Acta Mater, 2014, 79: 108–116
13 Liu T W , Xian X B, Wu S, et al. Properties of TiN films on uranium surface by arc ion plating under different bias voltages. Rare Met Mater Eng, 2006, 35: 1437–1440
14 Liang J C, Zhou W P, Zhang F G, et al. Influence of target on microstructure and mechanical behavior TiAlN coatings. Chin J Vac Sci Tech, 2014, 34: 714–719
15 Yu D H , Wang C Y, Cheng X L, et al. Microstructure and properties of TiAlSiN coatings prepared by hybrid PVD technology. Thin Solid Films, 2009, 517: 4950–4955
16 Ji F, Xue S B, Liu S, et al. Measurement of creep stress exponent of Zn-Al filler metal at room temperature by using nanoindentation. Trans China Weld Inst, 2013, 34: 75–79
17 Recco A A C, Viafara C C, Sinatora A, et al. Energy dissipation in depth-sensing indentation as a characteristic of the nanoscratch behaviour of coatings. Wear, 2009, 267: 1146–1152
18 Wang F J, Qian Y Y, Ma X. Measurement of mechanical properties of Sn-Ag-Cu bulk solder BGA solder joint using nanoindentation. Acta Sinica, 2005, 41: 775–779
19 Peng J, Long Z L, Wei H Q, et al. Creep behavior of a Fe-based bulk amorphous alloy using nanoindentation. Acta Phys Sinica, 2009, 58: 4059–4065
20 Oliver W C, Pharr G M. An improved technique for determining hardness and elastic modulus using load and displacement sensing indentation experiment. J Mater Res, 1992, 7: 1564–1583
21 Yetna M N, Chicot D, Ndjaka J.M, et al. A criterion to identify sinking-in and piling-up indentation of materials. Int J Mech Sci, 2015, 90: 145–150
22 Han C F, Lin J. Modeling to evaluate the contact areas of hard materials during the nano-indentatio en-Finn tests. Sensor Actuat A-Phys, 2008, 147: 229–241
23 Kang S K, Kim Y C, Lee J W, et al. Effect of contact angle on contact morphology and Vickers hardness measurement in instrumented indentation testing. Int J Mech Sci, 2014, 85: 104–109
24 Ricardo D T, Paulo C S J, Cleomar S, et al. Influence of the nitriding and TiAlN/TiN coating thickness on the sliding wear behavior of duplex treated AISI H13 steel. Surf Coat Tech, 2010, 205: 1381–1385